eXPRESS Polymer Letters Vol.6, No.2 (2012) 169–176
Available online at www.expresspolymlett.com
DOI: 10.3144/expresspolymlett.2012.18

Formation mechanism of porous hollow SnO_2 nanofibers prepared by one-step electrospinning

X. Xia[1,2], *X. J. Dong*[1], *Q. F. Wei*[1*], *Y. B. Cai*[1], *K. Y. Lu*[3]

[1]Key Laboratory of Eco-textiles, Jiangnan University, 214122 Wuxi, People's Republic of China
[2]Xinjiang University, Xinjiang, 830046 Wulumuqi, People's Republic of China
[3]State Key Laboratory of Food Science and Techology, 214122 Wuxi, People's Republic of China

Received 27 June 2011; accepted in revised form 16 September 2011

Abstract. The present study investigates the formation mechanism of hollow SnO_2 nanofibers and the form of nanograin growth in nanofibers. SnO_2 hollow nanofibers were fabricated by directly annealing electrospun polyvinylpyrrolidone (PVP)/Sn precursor composite nanofibers. In this approach, an appropriate proportion of PVP/Sn precursor with co-solvents established a system to form core/shell PVP/Sn precursor structure, and then PVP was decomposed quickly which acted as sacrificial template to keep fibrous structure and there existed a Sn precursor/SnO_2 concentration gradient to form hollow SnO_2 nanofibers due to the Kirkendall effect and surface diffusion during the calcination process. This deduction was also confirmed by experimental observations using transmission electron microscopy. The study suggested that surface diffusion and lattice diffusion were both driving force for nanograin growth on the surface of SnO_2 nanofibers. As supporting evidence, the tetragonal rutile SnO_2 hollow nanofibers were also characterized by X-ray diffraction, scanning electron microscopy and Brunauer–Emmett–Teller analysis.

Keywords: *nanomaterials, SnO_2, hollow nanofiber, electrospinning, Kirkendall effect*

1. Introduction

SnO_2 is an oxide semiconductor with many applications in the areas of sensors [1, 2] and optoelectronic devices [3, 4]. The properties of SnO_2 in various forms such as nanoparticles [5], nanowires [6], nanobelts [7] and other one-dimensional nanostructures have been extensively studied. In comparison with solid one-dimensional nanomaterials, nanotubes gain the advantages in practical applications to catalysts and gas sensors, owing to their higher surface-to-volume ratio. Generally, the conventional methods for preparing SnO_2 nanotubes by self-assembly [8] and templates directed process [9] often suffer from strict synthesis conditions or tedious procedures. Electrospinning has been considered as a simple and efficient method for fabricating nanofibers including organic and inorganic materials. However, templates and the co-electrospinning technique [10] had to be used for forming inorganic nanotubes. Herein, one-step method for the fabrication of SnO_2 hollow nanofibers by directly annealing electrospun composite nanofibers was proposed in this work. Though Cheng *et al.* and Li's group have reported the fabrication of hollow TiO_2 nanofibers [11] and porous SnO_2 nanofibers [12] by the similar technique, respectively; there has been no report about the detailed analysis on the formation mechanism and the growth behavior of nanograins on the nanofiber surface. Generally, the formation mechanism of hollow nanofibers which were fabricated via the electrospinning process, followed by heat treatment is attributed to the decomposition of sacrificial template of organic polymer at the high temperature.

*Corresponding author, e-mail: qfwei@jiangnan.edu.cn
© BME-PT

In this work, a systematic investigation into the structures of as-spun nanofiber, the effect of calcination and crystallite growth was conducted for understanding the formation mechanism of SnO_2 hollow nanofibers. In addition, the growth kinetics SnO_2 nanograin in individual nanofiber was also proposed.

2. Experimental

2.1. Preparation of porous hollow SnO_2 nanofibers

Stannic chloride pentahydrate ($SnCl_4 \cdot 5H_2O$), ethanol and N,N-dimethylformamide (DMF) were purchased from Sinopharm Chemical Reagents Co., Shanghai, China. Polyvinylpyrrolidone (PVP, M_w = 1300 000 g·mol^{-1}) was supplied by Qi Fuqin Materials Technology Co., LTD. Shanghai, China. Transparent spinning solution was prepared by adding 3 g of $SnCl_4 \cdot 5H_2O$ into 10 wt% PVP in ethanol/DMF solvent mixture (weight ratio 1:1), and the weight ratio of PVP and $SnCl_4 \cdot 5H_2O$ was also 1:1, followed by magnetic stirring at ambient temperature. Subsequently, the solution was electrospun from the stainless steel needle with an electrostatic voltage of 18 kV, and formed a fibrous mat on a collector of aluminum foil. The distance between the needle and collector was 22 cm. The electrospun fibers were then calcinated at 600°C for 3 hrs with a heating rate of 0.5°C/min.

2.2. Structural observations

The structures of the electrospun nanofibers were observed by a scanning electron microscope (SEM; Hitachi S-4800, Japan) and a high-resolution transmission electron microscope (TEM; JEOL-2100, Japan). The electrospinning specimens were sputter coated with gold before SEM observation, while the SnO_2 nanofibers were examined without any further treatment. For TEM observation, the electrospun composited nanofibers were directly collected on the copper grids for about 30 seconds during electrospinning, while the SnO_2 nanofibers were dispersed ultrasonically in ethanol, and then transferred onto copper grids before TEM observation.

2.3. XRD and TGA analyses

The crystal structure analysis was performed on D8 Advance X-ray diffraction (Bruker AXS, Germany), over the 2θ range of 10–80º. Thermogravimetric studies were carried out using an SDT 851 thermal analyzer system (Mettler, Germany) at a heating rate of 10°C/min.

2.4. Surface area measurement

The porosity and specific surface areas of the electrospun fibers were measured by N_2 adsorption-desorption isotherm at 77 K with a Micromeritics NOVA2000e apparatus (Quantachrome, America).

3. Results and discussion

3.1. Structure observations

Figure 1 demonstrates the morphologies of the electrospun nanofibers before and after calcination at 600°C. The as-spun PVP/SnO_2 nanofibers have a variable diameter ranged between 50 and 300 nm and form a self-supporting network, as shown in Figure 1a. The TEM image clearly reveals the core-shell structure with clear boundary of a phase sepa-

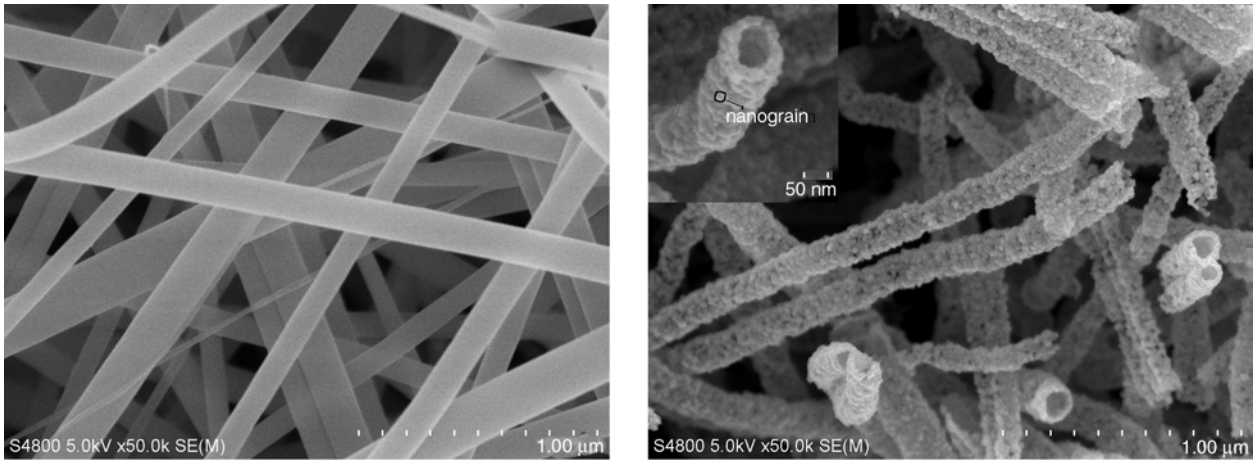

Figure 1. SEM images of (a) as- spun PVP/SnO_2 nanofibers (b) porous hollow SnO_2 nanofibers after calcination at 600°C

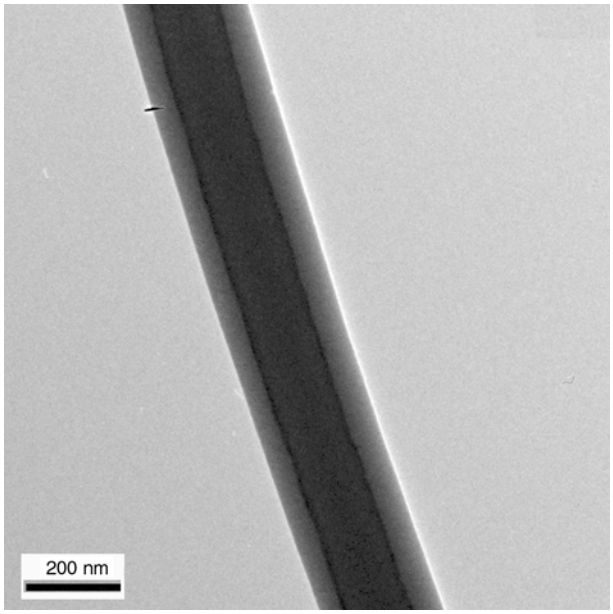

Figure 2. TEM images of as-spun PVP/SnO_2 nanofibers at room temperature

ration between PVP and Sn precursor, as presented in Figure 2.

Figure 1b shows the image of SnO_2 nanofibers obtained by the calcination treatment of as-spun core-shell PVP/SnO_2 nanofibers. It can be clearly seen that these fibers have a tubular structure with dense shells, which consist of nanograins of approximately 17 nm in diameter, as revealed in Figure 1b. Besides SnO_2 nanofibers have a relatively uniform diameter, the outer diameter of the hollow fibers is decreased compared to that of the as-spun PVP/SnO_2 fibers shown in Figure 1a.

3.2. Formation of porous hollow SnO_2 nanofibers

The forming process of hollow SnO_2 nanofibers experiences 5 stages during electrospinning and calcination. Based on the TEM observations combined TGA/DTGA analysis, the formation process of SnO_2 nanofibrous structures can be traced. At the initial stage during electrospinning, the core-shell fibers are fabricated via single capillary electrospinning from homogeneous polymer-sol-double solvents system due to solvent evaporation and rapid phase separation [13]. Various factors may have strong influences on the morphology of the electrospun fibers due to the complexity of hydrolysis and condensation reactions during the gelation of sol as well as the process of fiber formation. The hydrolysis reaction of $SnCl_4$ in water is schematically illustrated in Figure 3. In this work, excessive ethanol was applied to prepare Sn precursor but insufficient H_2O was used to make it partially hydrolyzed. Thus, the polymerization and polycondensation reactions of tin dioxide could be limited to a very low level. Furthermore, a kind of more volatile solvent ethanol evaporates rapidly at the edge of the fiber and a contrary concentration gradient of ethanol and DMF along the radial direction of the fiber will be formed during electrospinning. Especially, ethanol, the 50% weight ratio of solvents, which was used for preparation tin alkoxide, on the surface of the fibers is too little to form large solvent-rich regions during the phase separation because of the rapid evaporation. The high molecular weight PVP and high concentration solution contribute to retain less ethanol to form porous surface as well. So the smooth and compact surface without any porous structures can be observation by TEM, as revealed in Figure 2. At the same time, Sn precursor in nature has a very much higher solubility in ethanol than in PVP [14]. So, it would diffuse from the surface to the core of the fiber. As a result, Sn precursor tends to congre-

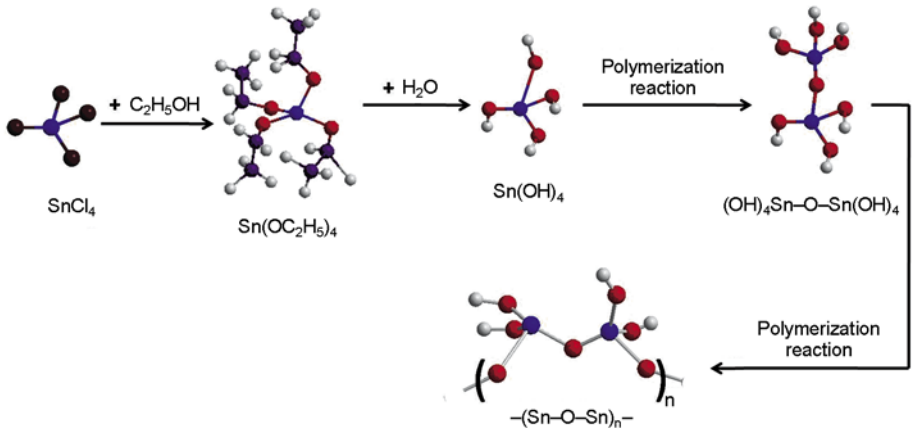

Figure 3. Schematic illustration of the hydrolytic–polymeric reaction of $SnCl_4 \cdot 5H_2O$. Tin, blue; oxygen, red; carbon, purple; hydrogen, white; chlorine, brown.

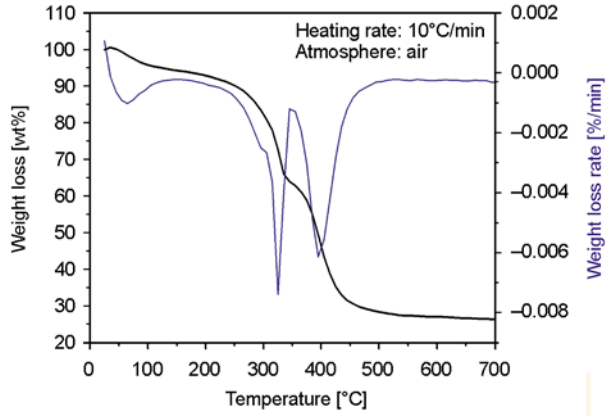

Figure 4. TGA-DTGA graph of thermal decomposition of electrospun PVP/SnO_2 composite nanofibers

gate at the center of the fiber by the driving force of the concentration gradient of ethanol, resulting in a clear core/shell structure.

At the second stage, the first weight loss stage which coincides with the decomposition of PVP chain at the temperature around 280 to 330ºC occurs [15], as shown in Figure 4. The core-shell nanofibers still exist though the diameter of fiber decreases and the boundaries between core and shell are blurred, as indicated in Figure 5a. Eventually, the core-shell structure disappears after the second endothermic peak from 350–480ºC (Figure 4) due to the almost complete decomposition of PVP, in which the process

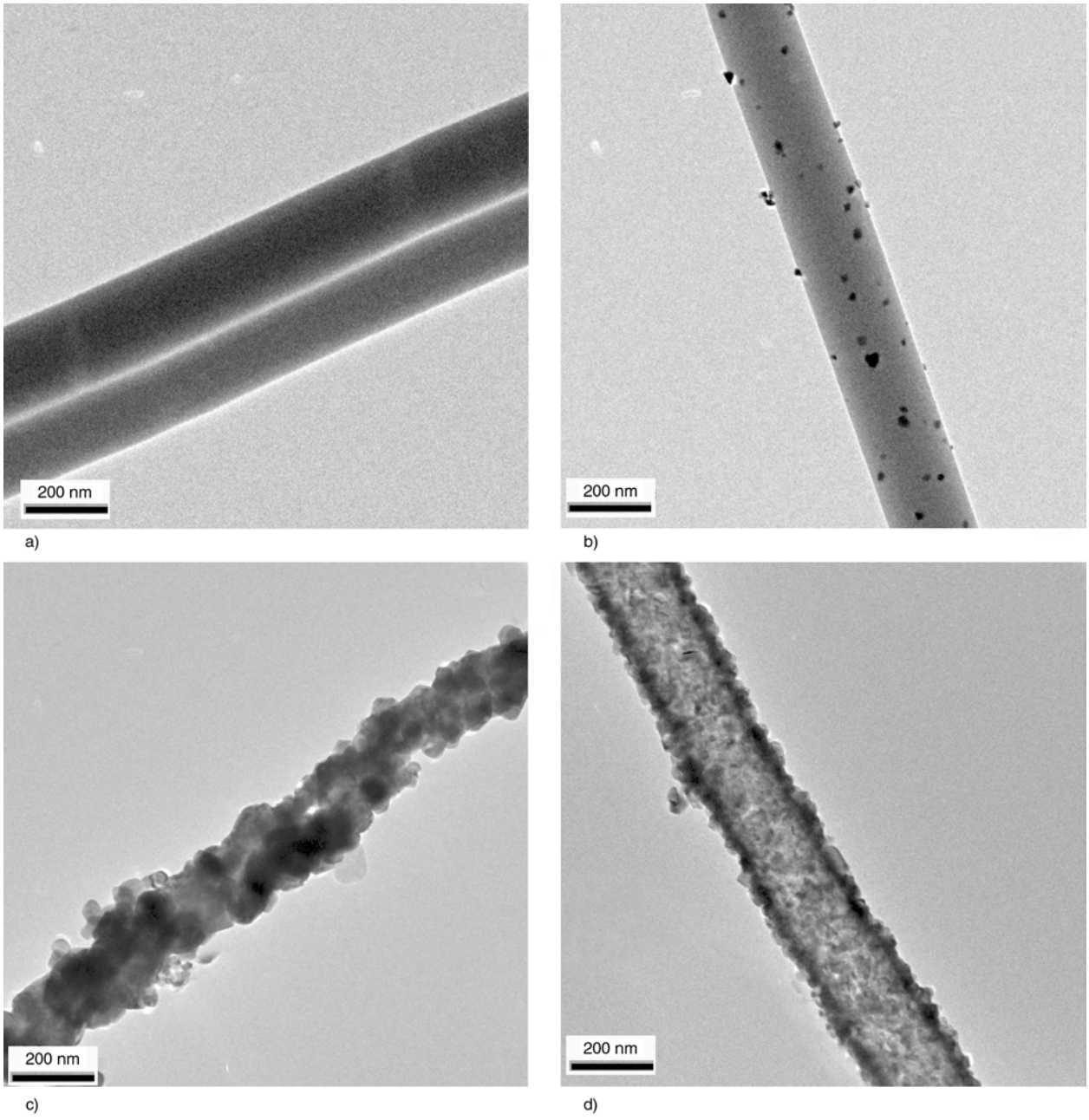

Figure 5. TEM images of PVP/SnO_2 nanofibers (a) calcined at 300ºC, (b) calcined at 400ºC, (c) calcined at 500ºC, (d) calcined at 600ºC

enters the third stage. At this stage, the Sn precursor on the surface region of the electrospun nanofibers is exposed to air, leading to the decomposition and oxidation of the precursor and resulted in the formation of SnO_2. Thus some small SnO_2 particles are presented on the surface whereas most Sn precursor inside the fibers remains unreacted due to the absence of oxygen, leading to solid fiber structure with particles on surface, as illustrated in Figure 5b. When the forming process enters the fourth stage which is a complicated transformation process including grain formation, grain growth and grain reorganization. Figure 5c may be one of morphological situation during this process. Nanograins are the main components to build solid body though the fibers appear to be irregular. Finally, the hollow SnO_2 nanofibers are formed with porous nanograins on the shell, as shown in Figure 5d

According to TEM observations of the hollow SnO_2 nanofibers formation, it is clearly revealed that PVP and Sn precursor are the main constituents of core-shell as-spun nanofibers. Then PVP is gradually decomposed during the calcination process. In this process, PVP plays the role of sacrificial template, which is the key effect to maintain fibrous structures. The decomposition of PVP, to some extent, reduces the final fiber diameters. The key mechanism responsible for the formation of hollow nanofibers is attributed to the interaction between Sn precursor and SnO_2 which will be discussed in the next section.

3.3. Analysis of formation mechanism

As mentioned above, the main components after the complete decomposition of PVP are some SnO_2 particles on the surface region and the massive Sn precursors in the core to form a concentration gradient, which lead to a Kirkendall effect [16]. Kirkendall effect is associated with the phenomenon of a considerable amount of compounds moving in or out of a sphere due to the diffusion coupled with different diffusion rates [17]. When the solid fiber consists of Sn precursor and SnO_2 (Figure 6a), the outward transport of fast-moving Sn precursor molecules (short as J_a in Figure 6) move through the oxide layer and a balancing inward flow of vacancies traverse to the vicinity of the Sn precursors and Sn precursors/SnO_2 mixture interface (*a*/*ab* interface) and vacancies assisted exchange of material depends on the way of bulk inter-diffusion, as illustrated in Figure 6b. Then, the voids are just like sinks to transfer the inward flux of vacancies ($J_c = J_a - J_b$) and the voids coalesce into bigger ones so as to touch the compound layer *ab*. Such new bridges are established as fast transport paths for the remaining Sn precursors (Figure 6c). At this stage, the surface diffusion takes over the dominant material transport process because the porous surface owns much lower apparent activation energy than those of bulk diffusion [18]. Sn precursors can be quickly oxidized at the surface of ab layer and redistribute themselves via fast surface diffusion, while the ab layer remains bulk inter-diffusion associated with Kirkendall effect until the whole Sn precursors turn into SnO_2. Therefore, SnO_2 stands on the shell and vacancies are continuously generated and flow inward to build a hollow core, as shown in Figure 6d. In all, the fibrous structure is established by PVP template and Kirkendall effect contributions to form hollow structure. Furthermore, surface diffusion also plays an important role to build hollow fibers.

The surface diffusion is also beneficial to the nano-sized grains growth. In the experiments, the annealing time (≤4 hrs) obeys the parabolic kinetic equation of grain growth for isothermal annealing as Equation (1):

$$D^m - D_0^m = Kt \tag{1}$$

where t is the annealing time, D is the average grain size after annealing for time t, D_0 is the initial grain size, m is the grain growth exponent, and K is a temperature dependent rate constant $=1.04 \cdot 10^{13}$ at 600ºC [19].

The average grain size after 3 hrs calcination is obtained by calculating the size of three intense peaks, (110), (101) and (211) of SnO_2 from XRD

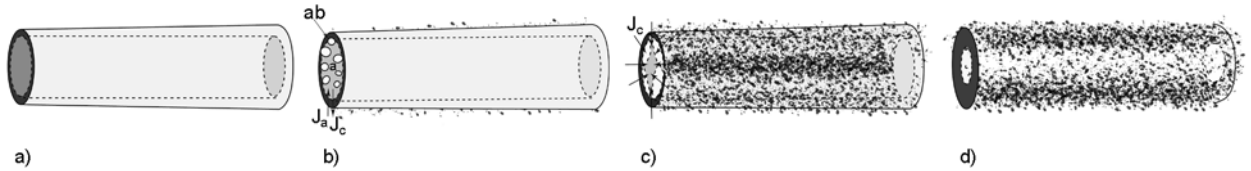

Figure 6. The model for hollow structure formation of SnO_2 nanofibers (see text for details)

patterns. When D_0 is neglected, the estimated m value is 13.2, which is inconsistent with the classical grain growth value (m = 2~4) [20], which means the grain growth of the nanograins observed in the individual nanofibers cannot be primarily ascribed by lattice diffusion in a pore controlled scheme. When the new bridges are established to transport the mass materials as mentioned above, the connection for lattice diffusion are broken and surface diffusion will enhance the local voids, meanwhile acts as the driving force for grain growth, leading to acceleration in the speed of coarse grains by the reduction of the free energy of the system. However, the growth kinetics of nanograins in hollow SnO_2 fibers is complicated and needs further investigation. Heating rate should be studied to control the morphology of fibers while using the temperature and duration of calcination as a tool to obtain desired nanograins on nanofiber surfaces have already been reported by Park *et al*. in Ref [20].

XRD patterns in Figure 7 confirm the formation of SnO_2 fibers. The fibers after calcination at 300ºC show a broad continuum indicating that the crystallization of tin oxide just starts at this temperature but not sufficient enough to produce the diffraction patterns. However, the XRD patterns of the fibers after calcination at 400ºC show the emergence of tetragonal rutile tin oxide crystals with distinct peaks due to the decomposition of PVP and oxidation of some Sn precursors on the fiber surface. The diffraction peaks become much sharper and well defined after calcination at 500 and 600ºC, without altering their positions but with high intensity because of better crystallization. All the diffraction peaks are indexed to the tetragonal rutile SnO_2, the only crystalline phase existing in the obtained nanofibers.

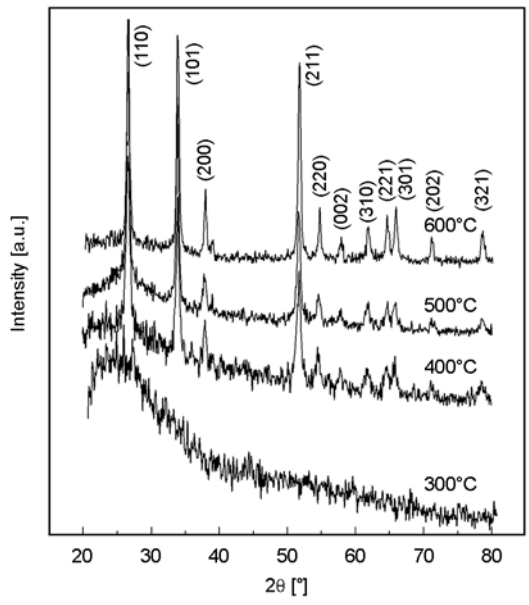

Figure 7. XRD patterns of SnO_2 nanofibres at different temperature

3.4. Surface areas

Brunauer–Emmett–Teller (BET) gas sorption measurement reveals the surface area of the hollow SnO_2 fibers. The N_2 adsorption–desorption isotherm curve of the porous SnO_2 fibers is shown in Figure 8. It exhibits the characteristic of mesopore structures, especially even owns an adsorption at high P/P_0, which was also reported as an aggregation of plate-like particles giving rise to slit-shaped pores [21]. The porous structure is confirmed by the SEM observations shown in Figure 1b. The average pore size in the porous SnO_2 fibers is approximately 16.2 nm, and the corresponding BET specific surface area is about 35.8 m^2/g (BJH method).

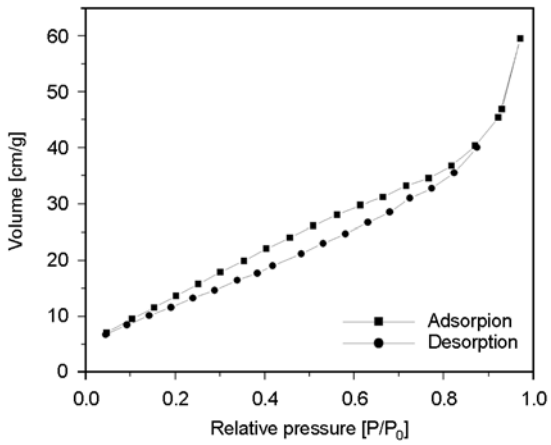

Figure 8. Nitrogen adsorption/desorption isotherms of the hollow SnO_2 nanofibers

4. Conclusions

In this work, porous hollow SnO_2 nanofibers were successfully prepared by electrospinning technique via a single capillary from PVP/Sn precursors/dual solvents system with calcination treatment. During the electrospinning process, a stringent component matching contributes to core-shell structure which provided advantages for preserving fibrous structures based on sacrificial PVP template. Hollow structures initiated by the Kirkendall effect owing to the concentration gradient of Sn precursors and SnO_2, suggesting that surface diffusion processes

might be the dominant mass flow mechanism responsible for the enlargement of the interior pores after initially formation induced by the Kirkendall effect. This deduction was also confirmed by the calculated grain growth value which was higher than the classical one, which means the grain growth mechanism occurred not only by the lattice diffusion but also through surface diffusion. This mechanism should also apply to the synthesys of other hollow nanofibers. The technique described here will be extendible to many other materials for fabricating such hollow inorganic nanofibers with potential applications in catalysis, microelectronics, and optics.

Acknowledgements

The research was supported by the specialized Research Fund for the Doctoral Program of higher education (No.20090093110004) and National Natural Science Foundation of China (No.51006046 and No.51163014).

References

[1] Song X., Qi Q., Zhang T., Wang C.: A humidity sensor based on KCl-doped SnO_2 nanofibers. Sensors and Actuators B: Chemical, **138**, 368–373 (2009). DOI: 10.1016/j.snb.2009.02.027

[2] Zhang Y., Li J. P., An G. M., He X.: Highly porous SnO_2 fibers by electrospinning and oxygen plasma etching and its ethanol-sensing properties. Sensors and Actuators B: Chemical, **144**, 43–48 (2010). DOI: 10.1016/j.snb.2009.10.012

[3] Zhang Z., Shao C., Li X., Zhang L., Xue H., Wang C., Liu Y.: Electrospun nanofibers of ZnO–SnO_2 heterojunction with high photocatalytic activity. Journal of Physical Chemistry C, **114**, 7920–7925 (2010). DOI: 10.1021/jp100262q

[4] Yang Z., Du G., Feng C., Li S., Chen Z., Zhang P., Guo Z., Yu X., Chen G., Huang S., Liu H.: Synthesis of uniform polycrystalline tin dioxide nanofibers and electrochemical application in lithium-ion batteries. Electrochimica Acta, **55**, 5485–5491 (2010). DOI: 10.1016/j.electacta.2010.04.045

[5] Gong S., Liu J., Xia J., Quan L., Liu H., Zhou D.: Gas sensing characteristics of SnO_2 thin films and analyses of sensor response by the gas diffusion theory. Materials Science and Engineering B: Advanced Functional Solid-State Materials, **164**, 85–90 (2009). DOI: 10.1016/j.mseb.2009.07.008

[6] Xu L., Dong B., Wang Y., Bai X., Liu Q., Song H.: Electrospinning preparation and room temperature gas sensing properties of porous In_2O_3 nanotubes and nanowires. Sensors and Actuators B: Chemical, **147**, 531–538 (2010). DOI: 10.1016/j.snb.2010.04.003

[7] Soares A. J., Perry R. J.: Modeling and simulation of a single tin dioxide nanobelt FET for chemical sensors. IEEE Sensors Journal, **10**, 235–242 (2010). DOI: 10.1109/JSEN.2009.2032154

[8] Qiu Y., Chen P., Liu M.: Evolution of various porphyrin nanostructures via an oil/aqueous medium: Controlled self-assembly, further organization, and supramolecular chirality. Journal of the American Chemical Society, **132**, 9644–9652 (2010). DOI: 10.1021/ja1001967

[9] Park J. Y., Choi S-W., Kim S. S.: A synthesis and sensing application of hollow ZnO nanofibers with uniform wall thicknesses grown using polymer templates. Nanotechnology, **21**, 475601 (2010). DOI: 10.1088/0957-4484/21/47/475601

[10] Chen H., Wang N., Di J., Zhao Y., Song Y., Jiang L.: Nanowire-in-microtube structured core/shell fibers via multifluidic coaxial electrospinning. Langmuir, **26**, 11291–11296 (2010). DOI: 10.1021/la100611f

[11] Cheng Y., Huang W., Zhang Y., Zhu L., Liu Y., Fan X., Cao X.: Preparation of TiO_2 hollow nanofibers by electrospining combined with sol–gel process. CrystEngComm, **12**, 2256–2260 (2010). DOI: 10.1039/b922564a

[12] Li L., Yin X., Liu S., Wang Y., Chen L., Wang T.: Electrospun porous SnO_2 nanotubes as high capacity anode materials for lithium ion batteries. Electrochemistry Communications, **12**, 1383–1386 (2010). DOI: 10.1016/j.elecom.2010.07.026

[13] Zhang K., Wang X., Yang Y., Wang L., Zhu M., Hsiao B., Chu B.: Aligned and molecularly oriented semihollow ultrafine polymer fiber yarns by a facile method. Journal of Polymer Science Part B: Polymer Physics, **48**, 1118–1125 (2010). DOI: 10.1002/polb.22003

[14] Wang W., Zhou J., Zhang S., Song J., Duan H., Zhou M., Gong C., Bao Z., Lu B., Li X., Lan W., Xie E.: A novel method to fabricate silicananotubes based on phase separation effect. Journal of Materials Chemistry, **20**, 9068–9072 (2010). DOI: 10.1039/C0JM02120B

[15] Loría-Bastarrachea M. I., Herrera-Kao W., Cauich-Rodríguez J. V., Cervantes-Uc J. M., Vázquez-Torres H., Ávila-Ortega A.: A TG/FTIR study on the thermal degradation of poly(vinyl pyrrolidone). Journal of Thermal Analysis and Calorimetry, **104**, 737–742 (2010). DOI: 10.1007/s10973-010-1061-9

[16] Yin Y., Rioux R. M., Erdonmez C. K., Hughes S., Somorjai G. A., Alivisatos A. P.: Formation of hollow nanocrystals through the nanoscale Kirkendall effect. Science, **304**, 711–714 (2004).
DOI: 10.1126/science.1096566

[17] Kong J., Tan H. R., Tan S. Y., Li F., Wong S. Y., Li X., Lu X.: A generic approach for preparing core–shell carbon–metal oxide nanofibers: Morphological evolution and its mechanism. Chemical Communications, **46**, 8773–8775 (2010).
DOI: 10.1039/C0CC03006F

[18] Fan H. J., Knez M., Scholz R., Hesse D., Nielsch K., Zacharias M., Gösele U.: Influence of surface diffusion on the formation of hollow nanostructures induced by the Kirkendall effect: The basic concept. Nano Letters, **7**, 993–997 (2007).
DOI: 10.1021/nl070026p

[19] Lai J. K. L., Shek C. H., Lin G. M.: Grain growth kinetics of nanocrystalline SnO_2 for long-term isothermal annealing. Scripta Materialia, **49**, 441–446 (2003).
DOI: 10.1016/S1359-6462(03)00296-3

[20] Park J. Y., Asokan K., Choi S-W., Kim S. S.: Growth kinetics of nanograins in SnO_2 fibers and size dependent sensing properties. Sensors and Actuators B: Chemical, **152**, 254–260 (2011).
DOI: 10.1016/j.snb.2010.12.017

[21] Sing K. S. W., Everett D. H., Haul R. A. W., Moscou L., Pierotti R. A., Rouquérol J., Siemieniewska T.: Reporting physisorption data for gas/solid systems with special reference to the determination of surface area and porosity. Pure and Applied Chemistry, **57**, 603–619 (1985).
DOI: 10.1351/pac198557040603